# Compression of Dynamic Medical CT Data Using Motion Compensated Wavelet Lifting with Denoised Update

Daniela Lanz, Jürgen Seiler, Karina Jaskolka, and André Kaup
Multimedia Communications and Signal Processing
Friedrich-Alexander-Universität Erlangen-Nürnberg (FAU)
Cauerstr. 7, 91058 Erlangen, Germany
Email: Daniela.Lanz,Juergen.Seiler,Karina.Jaskolka,Andre.Kaup@FAU.de



***Abstract*—For the lossless compression of dynamic 3-D+t volumes as produced by medical devices like Computed Tomography, various coding schemes can be applied. This paper shows that 3-D subband coding outperforms lossless HEVC coding and additionally provides a scalable representation, which is often required in telemedicine applications. However, the resulting lowpass subband, which shall be used as a downscaled representative of the whole original sequence, contains a lot of ghosting artifacts. This can be alleviated by incorporating motion compensation methods into the subband coder. This results in a high quality lowpass subband but also leads to a lower compression ratio. In order to cope with this, we introduce a new approach for improving the compression efficiency of compensated 3-D wavelet lifting by performing denoising in the update step. We are able to reduce the file size of the lowpass subband by up to $1.64\%$, while the lowpass subband is still applicable for being used as a downscaled representative of the whole original sequence.**

## I. Introduction

In the daily medical routine, dynamic volume data provide a good basis for analyses and predictions of spatio-temporal movements of particular parts of the human body. Fig. 1 shows the principal structure of a 3-D+t volume from Computed Tomography (CT). It consists of $T$ temporally equidistant 3-D volumes of size $X \times Y \times Z$. Due to the high temporal and spatial resolution, dynamic volumes can get very large, which makes storing and archiving them in a lossless manner impractical. Additionally, for telemedicine applications a scalable representation is often required that allows for tasks like browsing and fast previewing [1]. Moreover, CT data contain a lot of sensor noise. This is caused by the radiation which has to be kept low to reduce the risks for the patients as well as the short acquisition time which is kept as low as possible to avoid motion artifacts. Further, medical CT data have a higher bit depth than natural video sequences, namely 12 bits per pixel. Therefore, an efficient coding scheme is required.

Common video codecs are mainly designed for temporal 8-bit video sequences originating from the entertainment industry. One way to apply them on medical 12-bit 3-D+t data is to generate a single sequence over $t$ for every slice position $z$, resulting in $Z$ temporal sequences. In Fig. 1, the resulting sequence for slice position $z = 3$ is highlighted. Each

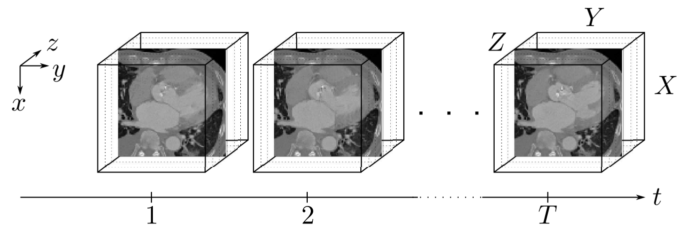


Fig. 1: Example of a dynamic medical data set: The sketch shows a 3-D+t CT volume of a thorax consisting of subsequent 3-D volumes over time $t$.

temporal sequence can be compressed using common video coding schemes under the condition of lossless compression and adaption of the range of the bit depth.

The HEVC standard [2], which describes a motion compensated predictive coder, is mainly applied for the efficient coding of video sequences. By choosing the *Lowdelay Main RExt* configuration and lossless mode, it is possible to apply HEVC also to medical sequences. An alternative coding scheme to predictive coding is represented by 3-D subband coding (SBC). Incorporating motion compensation (MC) methods into the subband coder is called Motion Compensated Temporal Filtering (MCTF) [3].

In [4], dynamic volume data is compressed by performing one Haar wavelet transform (WT) in temporal direction. This WT is performed in a simple SBC coder and in an MCTF coder with mesh-based MC. In both cases, the resulting subbands are coded losslessly using the wavelet-based volume coder JPEG 2000 [5] with four spatial decompositions steps.

Fig. 2 shows the resulting compression ratios of the above mentioned coders for medical as well as natural sequences. For the HEVC codec, the latest test model HM-16.16 was used. The medical sequences *Thorax1-3* originate from a 3-D+t CT data set at slice positions $z = 1, 2, 3$. The content of this volume can exemplarily be seen in Fig. 1 and describes a beating heart. The natural sequences consist of three HEVC-specific *ClassD* sequences [6]. As the medical sequences comprise luminance information only, all sequences are used in 4:0:0 color sub-sampling format for a fair comparison.

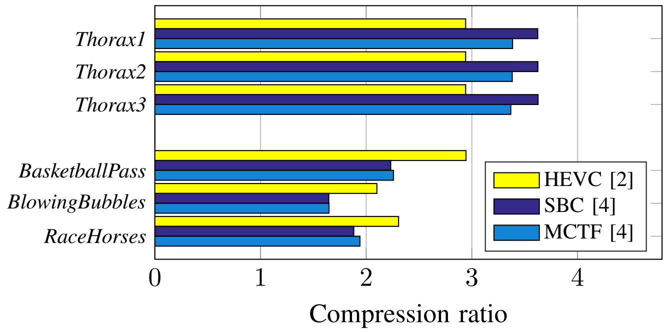


Fig. 2: Compression ratio resulting from HEVC, SBC, and mesh-based MCTF for medical (top) as well as natural sequences (bottom).

As can be seen in Fig. 2, HEVC reaches good compression ratios for natural sequences, but performs relatively less efficient for CT data. Apart from this, HEVC offers no scalable representation for the original volume. In contrast, SBC performs better than HEVC on medical CT data and additionally provides scalability features. However, SBC causes ghosting artifacts in the lowpass (LP) subband due to temporal displacements in the sequence. Thus, SBC is not recommended if the LP subband is to be used as a downscaled representative of the whole original sequence. MCTF performs not as well as SBC regarding the compression efficiency of medical CT data, but provides a high quality LP subband. Accordingly, MCTF results in a proper scalable representation for telemedicine applications.

To improve the compression efficiency of MCTF, we propose to apply denoising in the update step. With this, we avoid warping noise from the highpass (HP) subband to the LP subband. This novel step in the context of compensated wavelet lifting leads to a lower entropy in the LP subband and the compression ratio can be increased. By applying adequate filters for denoising, the compression ratio rises while the suitability of the LP subband for telemedicine applications is preserved at the same time.

After a short recap of compensated wavelet lifting in Section II, Section III provides a detailed description of the proposed method, followed by the simulation results in Section IV. In Section V we give a short conclusion and outlook.

## II. Compensated Wavelet Lifting

An efficient implementation of the discrete WT, named lifting structure, was proposed by Swelden [7]. The first step is a decomposition of the input video signal into even- and odd-indexed frames $f_{2t}$ and $f_{2t-1}$. In a prediction step, the odd frames are predicted and subtracted from the even frames, resulting in the HP frames. Then, in an update step, the HP frames are filtered and added back to the odd frames, resulting in the LP frames. Fig. 3 shows a block diagram of the lifting structure. The temporal HP and LP frames are generated by

$$\mathrm{HP}_t = f_{2t} - P(f_{2t-1}) \tag{1}$$
$$\mathrm{LP}_t = f_{2t-1} + U(\mathrm{HP}_t), \tag{2}$$

where $P(\cdot)$ and $U(\cdot)$ describe the prediction and update operators respectively. In the prediction step, MC is usually done to avoid ghosting artifacts in the LP frames that are caused by temporal displacements in the sequence [8]. This MC has to be inverted in the update step.

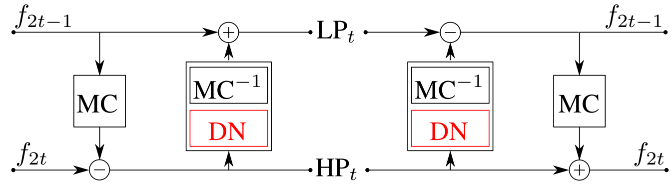


Fig. 3: Block diagram of the lifting structure containing the proposed denoising (DN) filter at both encoder (left) and decoder side (right).

However, while the appearance of ghosting artifacts is reduced by MC, the noise variance of the single subbands is increased. Structural information as well as noise is warped from one frame to the other by the prediction and update operators. As described in [9], this leads to a higher overall entropy, so the required number of bits for coding the subbands will also rise.

One possibility to reduce the increase of the noise variance in the LP frames is to skip the update step entirely. This results in the so-called Truncated WT, in which the LP frames are generated by subsampling the sequence by a factor of 2. However, apart from negative effects like temporal aliasing and temporal fluctuation in video quality as discussed in [10], the LP subband is not suitable anymore for telemedicine applications. An adequate downscaled representative should offer a high similarity to the odd- as well as to the even-indexed frames, which is not given by simply subsampling the original sequence.

## III. Compensated Wavelet Lifting with Denoised Update

To reduce the increase of the noise variance in the LP frames and thereby improving the compression efficiency of MCTF, we propose to apply denoising in the update step as shown in red in Fig. 3. Considering (1) and (2), the Wavelet Lifting with Denoised Update (WLDU) is described by

$$\mathrm{HP}_t = f_{2t} - \mathrm{MC}(f_{2t-1}) \tag{3}$$
$$\mathrm{LP}_t = f_{2t-1} + \mathrm{MC}^{-1}(\mathrm{DN}(\mathrm{HP}_t)). \tag{4}$$

Since the lifting scheme provides a flexible framework, $f_{2t}$ and $f_{2t-1}$ can be reconstructed without any loss if the denoising filter is also applied at the decoder side, resulting in

$$f_{2t-1} = \mathrm{LP}_t - \mathrm{MC}^{-1}(\mathrm{DN}(\mathrm{HP}_t)) \tag{5}$$
$$f_{2t} = \mathrm{HP}_t + \mathrm{MC}(f_{2t-1}). \tag{6}$$

These equations hold for any denoising filter without compromising the property of perfect reconstruction.

Under the assumption that the HP frames are zero-mean, an infinitely strong filter would only add zeros to the odd frames in the update step. This would correspond to the Truncated WT. In theory, the maximum achievable compression ratio of WLDU is hence bounded by the performance of the Truncated WT. Therefore, we apply a simple 2-D Gaussian filter in a first step so as to verify this theoretical bound of the compression ratio.

After that, we will apply more complex filters. To guarantee an accurate inverse MC in the update step, structural details in the HP frames shall be preserved while noisy structures caused by erroneous motion models and warping processes shall be blurred to avoid augmenting additional noise to the LP frames. In the context of video coding, various filters have been used for in-loop denoising of reference frames [11], which is why we will also apply them in our novel framework. These filters are the Adaptive Wiener Filter (AWF) [12], the Non-Local Means algorithm (NLM) [13], and Block Matching and 3-D Filtering (BM3D) [14]. In addition to these filters, we will apply Guided Image Filtering (GIF) [15].

All these algorithms are influenced by the filter strength $h$, which can be calculated by

$$h = \xi \cdot \sigma_n^2, \tag{7}$$

where $\sigma_n^2$ denotes the noise variance of the input image and $\xi$ describes an arbitrary parameter which optimizes the strength of denoising in order to improve the compression efficiency. By increasing $\xi$, the noise variance of the output image is decreased and according to [9], a better compression ratio can be reached.

Noise estimation is done at the encoder side. To guarantee lossless reconstruction, the estimated noise variance $\sigma_n^2$ has to be known at the decoder side. This can be assured by transmitting $\sigma_n^2$ as side information to the decoder or by estimating $\sigma_n^2$ at both the encoder and the decoder side. There exist different possibilities to perform noise estimation, which differ mainly with regard to the accuracy and the computational complexity. To avoid transmitting additional information to the decoder and to keep the decoder-side complexity low, we decided to estimate the noise variance by a low-complexity algorithm proposed in [16] at both the encoder and the decoder side.

By applying these filters in our novel framework of WLDU, we enforce a higher compression efficiency than MCTF, while the suitability of the LP subband for telemedicine applications is preserved.

## IV. Simulation Results

In our simulation setup, we use a 3-D+t medical CT data set[1] that describes a beating heart and comprises 10 time steps, each with 127 slices and a resolution of 512×512 pixels at 12 bits per sample. This results in 127 temporal sequences. The first three sequences correspond to the test

[1]The CT volume data set was kindly provided by Siemens Healthineers.

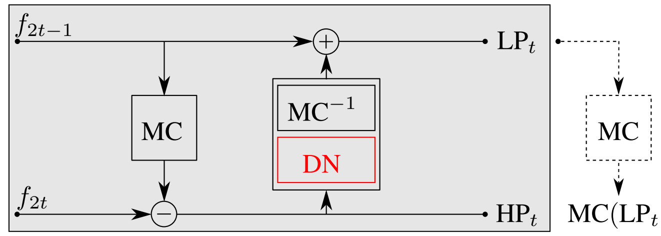


Fig. 4: Extended block diagram of the lifting structure illustrating the similarity of $\text{LP}_t$ to $f_{2t}$ and $f_{2t-1}$.

sequences *Thorax1-3* in Section I. We perform one Haar wavelet decomposition step with a mesh-based MC with and without the proposed denoising step. For the mesh-based MC, we use a grid size of 8×8 pixels. The subbands are compressed losslessly using the wavelet-based volume coder JPEG 2000. We use the OpenJPEG [17] implementation with four spatial wavelet decomposition steps in $xy$-direction.

### *A. Evaluation of the Quality of the Lowpass Subband*

Usually, the quality of the LP subband is measured by evaluating the similarity to the odd-indexed frames in terms of PSNR. However, in many applications the LP subband is to be used as a downscaled representative for the whole original sequence. Therefore, a high similarity between the LP frames and the even-indexed frames $f_{2t}$ should also be considered. As shown in Fig. 4, this can be done by warping each LP frame to the time step of the even-indexed frame and measure their similarity also in terms of PSNR. Since PSNR goes to infinity in case of perfect MC, it is not sufficient to calculate the average PSNR. Hence, for evaluating the LP frames of every time step with respect to both mentioned aspects, we suggest two different metrics:

- First we consider the variance of the error signal consisting of the even- and odd-indexed frames and their corresponding LP frames

$$\sigma_e^2 = \frac{1}{2}\left(\|f_{2t-1} - \text{LP}_t\|^2 + \|f_{2t} - \text{MC}(\text{LP}_t)\|^2\right). \tag{8}$$

  Then the quality of each lowpass frame $\text{LP}_t$ can be measured by

$$\text{PSNR}_{\text{LP}_t}[\text{dB}] = 10\log_{10}\frac{A_{\text{max}}^2}{\sigma_e^2}, \tag{9}$$

  where $A_{\text{max}}$ corresponds to the maximum possible amplitude of the signal.
- An alternative to PSNR is given by the Structural Similarity Index (SSIM) [18]. Since SSIM results in a range of [0,1], it is possible to calculate the average value regarding the similarity of each lowpass frame $\text{LP}_t$ to $f_{2t}$ and $f_{2t-1}$:

$$\text{SSIM}_{\text{LP}_t} = \frac{1}{2}\left(\text{SSIM}(f_{2t-1}, \text{LP}_t) + \right. \\ \left. + \text{SSIM}(f_{2t}, \text{MC}(\text{LP}_t))\right). \tag{10}$$

In the following sections, the term "quality of the lowpass

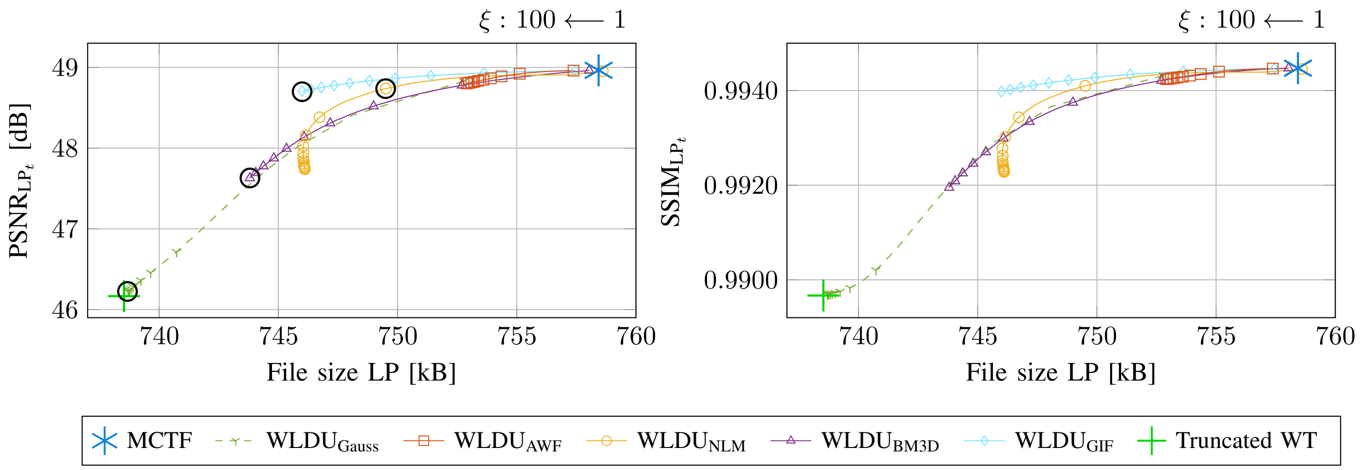


Fig. 5: PSNR$_{\mathrm{LP}_t}$ and SSIM$_{\mathrm{LP}_t}$ results compared against the file size of the LP frames in [kB]. The arrow above the diagrams shows the direction of the single curves for increasing values of the filter strength $h = \xi \cdot \sigma_n^2$. For better presentation, only every 10th value for $h$ is plotted.

subband" consequently describes a value calculated by one of these two metrics.

*B. Analysis of the Simulation Results*

Fig. 5 shows the PSNR$_{\mathrm{LP}_t}$ and SSIM$_{\mathrm{LP}_t}$ results over the file size of the LP subband in [kB] for all considered filter setups. We examine the influence of the filter strength $h$ by varying $\xi$ in a range of integer values from 1 to 100. The results are averaged over all frames of all sequences.

As mentioned in Section III, we verify the upper bound of the maximum achievable compression ratio by applying a simple 2-D Gaussian filter. The dashed green curve in Fig. 5 shows the development of WLDU$_{\mathrm{Gauss}}$ for increasing values of $h$. For high filter strengths the results are very close to the performance of the Truncated WT. However, the quality of the LP subband in terms of PSNR$_{\mathrm{LP}_t}$ as well as SSIM$_{\mathrm{LP}_t}$ decays rapidly, making it useless for telemedicine applications.

Any curve which lies above the curve of WLDU$_{\mathrm{Gauss}}$ results in a LP subband with a higher quality calculated by PSNR$_{\mathrm{LP}_t}$ or SSIM$_{\mathrm{LP}_t}$ that may be used in telemedicine applications. We are looking for a filter which keeps the quality of the LP subband at the level of MCTF for as long as possible. It should not decay until the upper bound for the compression ratio is almost achieved.

Therefore, we apply more complex denoising techniques as introduced in Section III. For the AWF, we use a window of 3×3 pixels. For the NLM algorithm, the support area has a size of 5×5 pixels and the neighborhood size is 3×3 pixels. The implementation used for BM3D is provided by [19]. GIF is applied under self-guidance, using HP$_t$ itself as the guidance image. The window used in GIF is of size 5×5 pixels.

According to Fig. 5, AWF seems not to be the right choice in the context of WLDU, since no gain regarding neither the compression ratio nor the quality calculated by PSNR$_{\mathrm{LP}_t}$ or SSIM$_{\mathrm{LP}_t}$ can be reached compared to WLDU$_{\mathrm{Gauss}}$. WLDU$_{\mathrm{BM3D}}$ has a quite high computational complexity but gives no significant advantage compared to WLDU$_{\mathrm{Gauss}}$. Therefore, it is also not suited for WLDU.

In contrast, by applying GIF and NLM as filters in the context of WLDU, we are able to reach higher compression ratios at nearly constant quality of the LP subband for small values of $h$. However, for higher filter strengths, WLDU$_{\mathrm{NLM}}$ completely fails in terms of PSNR$_{\mathrm{LP}_t}$ as well as SSIM$_{\mathrm{LP}_t}$. In contrast, WLDU$_{\mathrm{GIF}}$ keeps the quality of the LP subband at a high level even for high filter strengths. With WLDU$_{\mathrm{GIF}}$, we thus found a filter which fulfills the desired behavior: We achieve a higher compression efficiency of the LP subband at a quality close to MCTF with regard to both metrics PSNR$_{\mathrm{LP}_t}$ and SSIM$_{\mathrm{LP}_t}$.

For a closer examination, we choose one value in Fig. 5 that is good in a rate-distortion sense for each WLDU$_{\mathrm{NLM}}$, WLDU$_{\mathrm{BM3D}}$, and WLDU$_{\mathrm{GIF}}$. Additionally, we choose the lowest possible value which we can achieve by WLDU regarding the file size of the LP subband. This value belongs to WLDU$_{\mathrm{Gauss}}$. All these values are marked with black circles in Fig. 5. The corresponding values for the quality in terms of PSNR$_{\mathrm{LP}_t}$ and the file size of the LP subband can be found in Table I.

By applying WLDU$_{\mathrm{Gauss}}$, we can save 19.74 kB compared to MCTF, which corresponds to 2.60% bit rate savings. However, PSNR$_{\mathrm{LP}_t}$ amounts only to 46.22 dB. This loss of 2.74 dB constitutes the inability of the resulting LP subband for being used in telemedicine applications. In contrast, by applying the more complex filters, the quality of the LP subband in terms of PSNR$_{\mathrm{LP}_t}$ is significantly less degraded, while the file size can still be reduced by more than 1%. In particular, choosing WLDU$_{\mathrm{GIF}}$ saves 12.44 kB compared to MCTF. This corresponds to bit rate savings of 1.64% at a loss of only 0.25 dB regarding the quality of the LP subband. Consequently, the applicability of the LP subband to represent the whole original volume is preserved and the compression

TABLE I: File size and quality of the LP subband in terms of $\mathrm{PSNR}_{\mathrm{LP}_t}$ for certain values of Fig. 5. Absolute and relative differences against MCTF are also provided. The line printed in bold indicates the setup that we recommend for the given data set.

| | File size LP [kB] | Δ to MCTF | | $\mathrm{PSNR}_{\mathrm{LP}_t}$ [dB] | Δ to MCTF [dB] |
|---|---|---|---|---|---|
| | | absolute [kB] | relative [%] | | |
| MCTF | 758.43 | - | - | 48.96 | - |
| $\mathrm{WLDU}_{\mathrm{NLM}}$ | 749.51 | - 8.92 | -1.18 | 48.74 | -0.22 |
| **$\mathrm{WLDU}_{\mathrm{GIF}}$** | **745.99** | **-12.44** | **-1.64** | **48.71** | **-0.25** |
| $\mathrm{WLDU}_{\mathrm{BM3D}}$ | 743.80 | -14.63 | -1.92 | 47.63 | -1.33 |
| $\mathrm{WLDU}_{\mathrm{Gauss}}$ | 738.69 | -19.74 | -2.60 | 46.22 | -2.74 |
| Truncated WT | 738.53 | -19.90 | -2.62 | 46.17 | -2.79 |

efficiency is increased at the same time.

For very high filter strengths, however, the results stagnate for all applied filters. The theoretical upper bound of the maximum achievable compression ratio given by the Truncated WT cannot be reached by further increasing $\xi$. With larger neighborhood sizes for the single filters, a further compression would be possible. However, this would result in significantly lower values for $\mathrm{PSNR}_{\mathrm{LP}_t}$ as well as for $\mathrm{SSIM}_{\mathrm{LP}_t}$, which is not useful, if the LP subband is to be used as a downscaled representative.

## V. Conclusion

In this paper, a novel technique for improving the compression efficiency of MCTF at nearly constant quality of the LP subband in terms of $\mathrm{PSNR}_{\mathrm{LP}_t}$ as well as $\mathrm{SSIM}_{\mathrm{LP}_t}$ was proposed. After demonstrating that HEVC is not as efficient as SBC with regard to the compression of dynamic CT data, it was shown that SBC gives no satisfying scalable representation for use in telemedicine applications. Incorporating MC methods into the lifting structure of SBC was shown to result in a high quality LP subband, while suffering with regard to the compression efficiency. Therefore, we proposed to apply denoising in the update step, called WLDU. This novel approach preserves the suitability of the LP subband to be used as a downscaled representative of the whole original sequence and improves the compression efficiency at the same time. Further work aims at the investigation of optimum denoising filters and the suitability of deblocking filters for block-based MC.

## ACKNOWLEDGEMENT

We gratefully acknowledge that this work has been supported by the Deutsche Forschungsgemeinschaft (DFG) under contract number KA 926/4-3.

## References

[1] C. Doukas and I. Maglogiannis, "Adaptive transmission of medical image and video using scalable coding and context-aware wireless medical networks," *EURASIP J. Wirel. Commun. Netw.*, vol. 2008, pp. 25:1–25:12, Jan 2008.

[2] ITU-T and ISO/IEC, "High efficiency video coding (HEVC)," in *ITU-T Rec. H.265 and ISO/IEC FDIS 23008-2*, Dec 2016.

[3] J. R. Ohm, "Three-dimensional subband coding with motion compensation," *IEEE Transactions on Image Processing*, vol. 3, no. 5, pp. 559–571, Sep 1994.

[4] W. Schnurrer, N. Pallast, T. Richter, and A. Kaup, "Temporal scalability of dynamic volume data using mesh compensated wavelet lifting," *IEEE Transactions on Image Processing*, vol. 27, no. 1, pp. 419–431, 2018.

[5] ITU-T and ISO/IEC, "JPEG 2000 Image Coding System: Core Coding System," in *ITU-T Rec. T.800 and ISO/IEC 15444-1:2004*, Sep 2004.

[6] F. Bossen, "Common test conditions and software reference configurations," *Joint Collaborative Team on Video Coding (JCT-VC) of ITU-T SG16 WP3 and ISO/IEC JTC1/SC29/WG11*, Jan 2013.

[7] W. Sweldens, "Lifting scheme: a new philosophy in biorthogonal wavelet constructions," in *Proc. SPIE Int. Symp. on Optical Science, Engineering, and Instrumentation*, San Diego, CA, USA, Sep 1995, vol. 2569, pp. 68–79.

[8] A. Secker and D. Taubman, "Motion-compensated highly scalable video compression using an adaptive 3D wavelet transform based on lifting," in *Proc. IEEE Int. Conf. on Image Processing (ICIP)*, Thessaloniki, Greece, Oct 2001, vol. 2, pp. 1029–1032.

[9] W. Schnurrer, J. Seiler, M. Schöberl, and A. Kaup, "On the influence of clipping in lossless predictive and wavelet coding of noisy images," in *Picture Coding Symposium (PCS)*, Krakau, Polen, May 2012, pp. 185–188.

[10] N. Mehrseresht and D. Taubman, "Adaptively weighted update steps in motion compensated lifting based scalable video compression," in *Proc. IEEE Int. Conf. on Image Processing (ICIP)*, Barcelona, Spain, Sep 2003, vol. 3, pp. II–771–4.

[11] E. Wige, P. Amon, A. Hutter, and A. Kaup, "In-loop denoising of reference frames for lossless coding of noisy image sequences," in *Proc. IEEE Int. Conf. on Image Processing*, Hong Kong, Sep 2010, pp. 461–464.

[12] J. S. Lim, *Two-dimensional signal and image processing*, Englewood Cliffs, NJ, Prentice Hall, 1990.

[13] A. Buades, B. Coll, and J. M. Morel, "A non-local algorithm for image denoising," in *IEEE Computer Society Conference on Computer Vision and Pattern Recognition (CVPR)*, San Diego, CA, USA, June 2005, vol. 2, pp. 60–65 vol. 2.

[14] K. Dabov, A. Foi, V. Katkovnik, and K. Egiazarian, "Image denoising by sparse 3-D transform-domain collaborative filtering," *IEEE Transactions on Image Processing*, vol. 16, no. 8, pp. 2080–2095, Aug 2007.

[15] K. He, J. Sun, and X. Tang, *Guided Image Filtering*, pp. 1–14, Springer Berlin Heidelberg, Berlin, Heidelberg, 2010.

[16] J. Immerkær, "Fast noise variance estimation," *Computer Vision and Image Understanding*, vol. 64, no. 2, pp. 300 – 302, Sep 1996.

[17] A. Descampe, F. Devaux, H. Drolon, D. Janssens, and Y. Verschueren, "OpenJPEG 2.0.0," http://www.openjpeg.org, Nov 2012.

[18] Z. Wang, A. C. Bovik, H. R. Sheikh, and E. P. Simoncelli, "Image quality assessment: from error visibility to structural similarity," *IEEE Transactions on Image Processing*, vol. 13, no. 4, pp. 600–612, April 2004.

[19] K. Dabov, A. Foi, V. Katkovnik, and K. Egiazarian, "Image and video denoising by sparse 3-D transform-domain collaborative filtering," http://www.cs.tut.fi/ foi/GCF-BM3D/, 2007.